Available online at www.sciencedirect.com
SCIENCE DIRECT
Polymer 47 (2006) 4445–4453
polymer
www.elsevier.com/locate/polymer

Development of oriented morphology and tensile properties upon superdawing of solution-spun fibers of ultra-high molecular weight poly(acrylonitrile)

Daisuke Sawai, Yuya Fujii, Tetsuo Kanamoto *

Department of Applied Chemistry, Tokyo University of Science, Kagurazaka, Shinjuku-ku, Tokyo 162-8601, Japan

Received 8 September 2005; received in revised form 6 February 2006; accepted 17 March 2006
Available online 27 April 2006

Abstract

The uniaxial drawing of UHMW-PAN fibers spun from a dilute solution into methanol coagulation baths at different temperatures and the resultant structure and tensile properties of the drawn products were studied. Although the initial morphology of the fibers and the deformation mode in a lower draw ratio (DR_t) range were significantly dependent on the temperatures of the coagulation bath, the tensile properties at a given DR_t, as well as the maximum achieved ones, were comparable. Both the tensile modulus and strength increased steadily with the DR_t and reached 35 and 1.8 GPa, respectively, at the highest DR_t of $\sim$80. These tensile properties are among the highest ever reported for PAN fibers. The achievement of such high tensile properties for extremely drawn fibers is ascribed to the conformational changes of crystalline chains from the 3/1 helix to the planar-zigzag with increasing DR_t, the improvement in the uniformity of the fiber diameter along the fiber axis, and the decrease in fiber diameter. Indeed, the tensile strength of fibers prepared from a dilute solution and having comparable moduli increased with a decrease in the fiber diameters. The reciprocal of the strength was proportional to the square root of the diameter as suggested by the Griffith theory. Extrapolation to a zero diameter yielded an ultimate tensile strength of 2.4 ± 0.1 GPa for a fiber having a maximum achieved tensile modulus of 35 ± 1 GPa.

Keywords: Drawing of UHMW-PAN fibers; Tensile modulus and strength; Ultimate strength

1. Introduction

Poly(acrylonitrile) (PAN) is one of the most widely used polymers in the fiber industry. This polymer is commonly synthesized by radical polymerization; therefore, the atactic polymer obtained has no specific stereoregularity along the chain direction [1,2]. However, PAN is an unusual polymer in that even an atactic sample can crystallize. Therefore, the chain conformation of PAN is expected to be highly irregular [3–6]. The wide-angle X-ray diffraction (WAXD) patterns of oriented PAN fibers show a few sharp reflections on the equator, and only diffuse scatterings appear on the meridian and quadrants. Thus, the structure of PAN fibers is often assumed to be paracrystal [6–8] or mesophase [9] in which the chains have hexagonal or orthorhombic packing but there is no order along the chain axis.

This polymer has high cohesive energy density and fairly high chain stiffness due to the bulky nitrile groups with a large dipole [10]. Therefore, it has been assumed that PAN has low ductility [11]. However, following a gel-spinning/drawing technique to produce ultrahigh-molecular-weight (UHMW) polyethylene fibers with ultrahigh modulus and strength [12,13], this draw technique was applied to the preparation of acrylic fibers with improved mechanical properties [14]. Our previous studies [6,8,15] on the two-stage drawing of gel films of PAN demonstrated that high ductility and tensile properties could be achieved by optimizing the drawing variables, including the draw technique and conditions [6,8], the sample molecular weight [6], and incorporating a small amount of a comonomer [15]. The highest modulus of 28 GPa and strength of 1.5 GPa were achieved with an UHMW-PAN having the highest M_v of 2.3×10^6 at a draw ratio (DR) of around 120 [6]. This modulus value was significantly higher than those (23–24 GPa) [16,17] previously reported and close to an uncertain X-ray crystal modulus (28 GPa) [18].

It was shown that a PAN chain takes a 3/1 helical conformation (isotactic sequences) and a planar–zigzag

* Corresponding author. Tel.: +81 3 5228 8260; fax: +81 3 3235 2214.
E-mail address: tkanamot@ch.kagu.tus.ac.jp (T. Kanamoto).

0032-3861/$ - see front matter © 2006 Elsevier Ltd. All rights reserved.
doi:10.1016/j.polymer.2006.03.067

conformation (syndiotactic sequences) based on the wide-angle X-ray scattering on the meridian analyzed by computer simulations [19,20]. Furthermore, it was found that the planar–zigzag conformation increased with increasing the DR of the PAN fibers [6].

In this work, the following attempts have been made to study the ultimate tensile properties of PAN fibers: (1) to obtain a higher-molecular-weight sample [6,21,22]; (2) to improve the uniformity of the fiber diameter (or cross-sectional area); and (3) to make the fiber diameter smaller [23–26]. The development of the structure and tensile properties upon drawing of solution-spun fibers of UHMW-PAN was discussed to examine the effects of the above drawing variables on the tensile properties of the drawn products. The results obtained in this work were compared with those of the previous work on the drawing of gel films of UHMW-PAN [6] having rectangular cross sections.

2. Experimental section

2.1. PAN sample

The UHMW-PAN used in this work is the same as that used in a previous work on the ultradrawing of gel films by two-stage drawing. This UHMW-PAN was prepared by suspension polymerization of acrylonitrile using AIBN as an initiator and had a viscosity–average molecular-weight (M_v) of 2.3×10^6. The details of the polymerization and characterization are described in a previous paper [6].

2.2. Solution spinning

A polymer solution of 1 wt% was prepared by dissolving a requisite amount of UHMW-PAN in *N*,*N*′-dimethylformamide (DMF) at 100 °C. The solution was transferred to a cylinder with a diameter (L) of 10 mm equipped with a single-hole spinning die with a capillary diameter of $D=0.6$–2.0 mm. Thus, the cylinder diameter (L)/capillary diameter (D) = 5–17. The solution was cooled to 25 °C and kept at this temperature for 30 min before the initiation of dry-wet spinning. The solution was extruded through a spinning die into a methanol bath kept at room temperature (RT) (fiber-A) or −40 °C (fiber-B) through an air gap of 10 cm and collected on a bobbin moving at the same speed as the spinning. The spinning speed was approximately 10 m/min. The fibers obtained were extracted with methanol for 2 days at RT and then dried in vacuo to a constant weight. The diameters of as-spun fibers after drying were 0.10–0.25 mm, depending on the capillary diameters used. The as-spun fibers had no selective chain orientation as evaluated from their wide-angle X-ray diffraction (WAXD) patterns.

A gel film from the same UHMW-PAN was also prepared by quenching at 0 °C for 2 h of a 1 wt% solution of the UHMW-PAN in DMF at 100 °C contained in a stainless steel tray. The wet gel film obtained was extracted with methanol and then dried at room temperature (RT) in vacuo to a constant weight [6].

2.3. Drawing

In a previous study [6] on the ultradrawing of a gel film of the same UHMW-PAN prepared from 1 wt% solution in DMF, the film exhibited low ductility on the straight tensile draw. In an attempt to draw the gel film directly by a tensile force, a neck developed and further elongation led to failure of the sample. However, the gel film was ductile on solid-state coextrusion. The initially extrusion-drawn films with an extrusion draw ratio (EDR) of 16 exhibited high ductility on the second-stage tensile drawing to further improve the tensile properties. Further details of the two-stage drawing technique and the preparation conditions for the gel films of UHMW-PAN are described in previous papers [6,8,15].

In contrast to the gel film, the as-spun fibers studied in this work could be uniformly drawn directly by a tensile force. The first-stage tensile drawing of an as-spun fiber was made at 140 °C to a DR of 16 in an air oven equipped with an Orientec Tensilon tensile tester RTM-100 at constant crosshead speeds corresponding to an initial strain rate of 10 min^{-1}. Upon the first-stage drawing of an as-spun fiber, the thermal stability of the fiber increased, and the second-stage draw could be conducted at higher temperatures to obtain a higher draw. Thus, the second-stage tensile draw of the initially drawn fibers with a DR of 16 was made at 100–230 °C. The DR's for the first- and the second-stage draw were determined by the deformation of an ink mark preimprinted on the surface of a fiber. The total draw ratio (DR_t) after the second-stage draw was defined by DR_t = (first-stage DR × second-stage DR).

2.4. Characterization

WAXD patterns were recorded by a flat plate camera and diffractometer scans. Photographs were obtained with Cu Kα radiation generated at 40 kV and 25 mA on a Rigaku Geigerflex RAD-3A and monochromatized by a graphite crystal. The diffraction profiles were recorded with Ni-filtered Cu Kα radiation generated at 40 kV and 150 mA on a Rigaku Rotaflex 200 equipped with a diffractometer and a pulse height discriminator. The intensity was collected by step scans at 0.02° intervals in 2θ.

The crystalline chain orientation was evaluated by the Herman orientation function f_c [27]. The azimuthal intensity distribution was recorded by step scans at 0.1° intervals in the azimuthal angle, using a Rigaku fiber specimen holder with a first collimator with $\phi=0.3$ mm and a receiving slit of 1.8° (2θ direction) × 0.3° (azimuthal direction).

Scanning electron microscopic (SEM) observations of the free surface of a fiber and the fractured surface exposed by the fracture in liquid nitrogen (−196 °C) perpendicular to the fiber axis were made using a Hitachi S-5000 scanning electron microscope. SEM observations were also made to determine the diameters of the fibers. The magnification was calibrated using a grating replica of 2000 lines/mm.

The tensile modulus and strength on the fiber axis were measured at strain rates of 1×10^{-3} and 1×10^{-2} s^{-1}, respectively, at RT. The measurements were made at least

five times for a given sample. The modulus was determined from the initial slope of the stress/strain curve at low strain (< 0.1%). The cross sections of the fibers were nearly a perfect circle independently of the DR. Therefore, the average of the cross-sectional areas of a fiber and their variations along the fiber length were calculated from the fiber diameters determined by the SEM observations at 30 different positions along a 10 cm fiber. The sample lengths along the test direction were 200 and 30 mm for the tensile modulus and strength measurements, respectively.

3. Results and discussion

3.1. Ductility as a function of the draw temperature

In a previous study [8], the effects of the initial extrusion draw ratio (EDR) of an UHMW-PAN gel film on the deformation characteristics and ductility of the second-stage tensile draw were examined. When an extrudate of a low EDR $\leq$ 12 was tensile-drawn, the draw became unstable above a specific temperature, depending on the initial EDR. For an EDR $\geq$ 16, uniform deformation proceeded in the entire range of the T_d studied ($\leq$230 °C). Thus, extrudates with an EDR of 16 were chosen as a starting sample for further second-stage tensile draw.

For the tensile drawing of as-spun fibers, the maximum achieved DR was lower than 16 at a $T_d \leq 130$ °C. For the drawing at a $T_d > 160$ °C, uniform draw was not achieved for either of the fibers. Therefore, the first-stage draw of the fibers was made at 140 °C and a DR of 16.

Fig. 1 shows the maximum achieved DR ($DR_{t,max}$) as a function of the T_d for the second-stage tensile draw of fiber-A and fiber-B, which were previously tensile-drawn to a DR of 16 at 140 °C. The $DR_{t,max}$ observed for the second-stage draw of a gel film is also shown for comparison. The $DR_{t,max}$ for each of these samples increased markedly with T_d, reaching a maximum of 85–90 for the fibers and 145 for the gel film at a T_d of 200–210 °C. At yet higher T_d's, it decreased rapidly with increasing the T_d. The $DR_{t,max}$ values for the fibers were significantly lower than that of the gel film. The development of an oriented morphology upon drawing of the fibers will be discussed below based on the SEM observations and WAXD data. The results obtained in this work will also be compared with previous results of the two-stage drawing of a gel film [6,8].

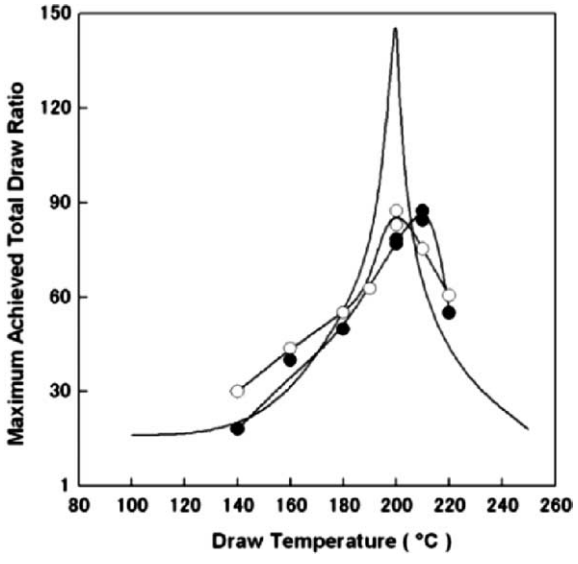

Fig. 1. Maximum achieved DR_t as a function of the second-stage draw temperature T_d for fiber-A (○) and fiber-B (●). The data for the two-stage draw of a gel film (—) [6] are also included for comparison.

3.2. Structural changes upon drawing

Fiber-A was translucent under visible light, whereas fiber-B was transparent. Fig. 2 shows SEM micrographs of the free surfaces (upper) and fractured surfaces (lower) of the as-spun fiber-A and fiber-B. SEM micrographs of a gel film prepared from a 1 wt% solution of the same UHMW-PAN in DMF are also shown for comparison. The SEM micrographs of the free surfaces on fiber-A and the gel film, both of which were translucent under visible light, showed fairly rough surfaces composed predominantly of granular particles with diameters of 40–70 nm, a few voids with similar diameters and a few smaller particles with diameters of ~20 nm. In contrast to these samples, the surface of fiber-B was composed of smaller particles (~20 nm) packed more closely than in the two other samples, resulting in a smoother surface with no voids.

The SEM micrographs of the fractured surfaces of these samples revealed significant differences in their interior morphologies reflecting their preparation conditions. The micrograph of the gel film showed that this sample was composed of lamellar-like textures with a width of 20–30 nm and a few granular particles and voids. The fractured surface of fiber-A, however, was predominantly composed of granular particles that had an average grain diameter of ~20 nm and a significantly smaller diameter than those at the surface region. Some lamellar-like textures and voids that were observed in the gel film were also present inside fiber-A. In contrast to these two samples, the fractured surface of fiber-B was composed of small grain particles (~20 nm) and no voids were found. These morphologies satisfactorily explain the translucence of the gel film and fiber-A and the transparency of fiber-B.

The fine textures and particle sizes of these fibers might be determined by the phase separation and subsequent solvent (DMF) extraction that occurred when the UHMW-PAN solutions were spun into methanol coagulation baths kept at different temperatures. When the UHMW-PAN solution was spun into a methanol bath kept at RT, the solvent (DMF) could be extracted faster than when using a methanol bath at a lower temperature of −40 °C. Rapid extraction of the solvent might produce voids penetrating from the interior to the surface of a fiber, whereas slow extraction of the solvent at a lower temperature (−40 °C) produced no voids, as observed by SEM micrographs. The gel film was prepared by a different process from that used for the fibers. For the preparation of a gel film, a hot solution (100 °C) in a stainless steel tray was quenched in ice water. As can be seen in the SEM micrograph of a fractured

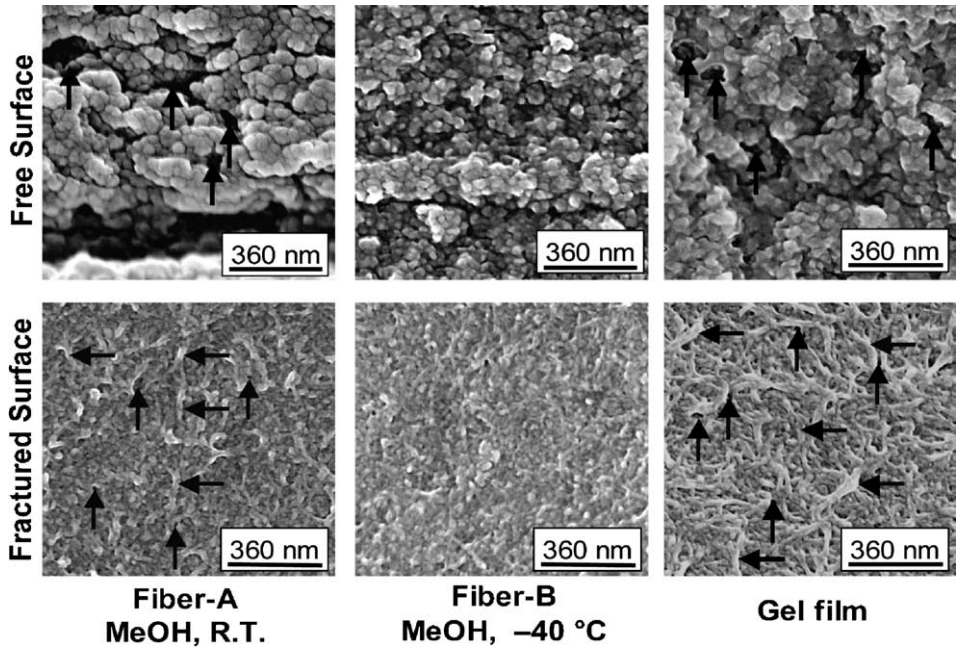

Fig. 2. SEM micrographs of free surfaces (upper) and fractured surfaces (lower) for two kinds of as-spun fibers, fiber-A and fiber-B. The micrographs of a gel film are also included for comparison. Lamellar-like textures and voids are shown by arrows, ← and ↑, respectively.

surface and would later be supported by the WAXD patterns, lamellar-like crystals developed in the gel film. Thus, the characteristics of these morphologies were controlled by the conditions for phase separation followed by solvent extraction.

Fig. 3 shows SEM micrographs which demonstrate the characteristic deformation behavior of (a) fiber-A and (b) fiber-B drawn up to an average strain of ~100% at a $T_d = 140$ °C. The deformation of fiber-A proceeded with the formation of a single neck for drawing at a $T_d \leq 140$ °C whereas at a $T_d > 150$ °C, the deformation proceeded with the formation of multiple necks. In contrast to fiber-A, fiber-B showed a macroscopically uniform deformation at $T_d = 140$ °C. For drawing at a $T_d < 130$ °C or a $T_d > 160$ °C, the achievable DR was lower than 16 for both fibers. The gel film was too brittle for a straight tensile draw; therefore, it was drawn by using the solid-state coextrusion technique [6]. Thus, the initial deformation behaviors upon tensile drawing of the two fibers coagulated in methanol at RT and −40 °C were markedly different reflecting the morphologies of the as-spun fibers (Fig. 2).

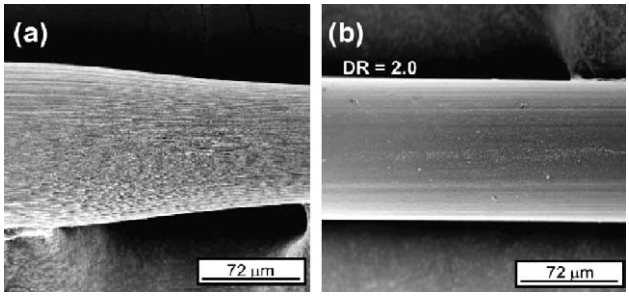

Fig. 3. SEM micrographs showing the characteristic deformation behaviors of the two kinds of fibers drawn at 140 °C. (a) Fiber-A showed neck deformation, whereas (b) fiber-B deformed uniformly.

Fig. 4 shows SEM micrographs of the draw ratio series from fiber-A and fiber-B with a DR ≤ 16 prepared by the first-stage draw at 140 °C. The DR's of necked portions were calculated from the diameters determined by SEM observations. The morphological changes at the initial stage of the deformation were markedly different between the two fibers corresponding to the macroscopically different deformation modes (Fig. 3). In fiber-A, which showed neck deformation macroscopically, the deformation proceeded through micro-neck formation initiated at the interfaces between grain particles, and microfibrils oriented along the draw direction were observed at a DR = 2. With increasing the DR, the grain particles further transformed into a fibrillar structure, the fibrils became longer, and the size and number of grain particles decreased. The voids that were observed in an as-spun fiber-A disappeared upon the draw. The fibers drawn to a DR above 16 showed a fibrous structure. In contrast to fiber-A, the deformation of the as-spun fiber-B proceeded uniformly during the tensile draw. The granular particles, which were initially present, gradually transformed into a fibrous structure with increasing the DR, and the transformation to a fibrous structure was almost completed at a DR of 16, as observed in fiber-A as well.

Fig. 5 shows the WAXD patterns for the draw ratio series prepared from fiber-A and fiber-B recorded with the incident X-ray beam perpendicular to the fiber axis. The WAXD patterns for a draw ratio series of a gel film are also shown for comparison. The as-spun fibers and gel film show random orientation. The WAXD patterns of the initial fibers show a broad (110, 200) reflection ring overlapped with fairly strong diffuse scatterings from disordered regions, whereas the gel

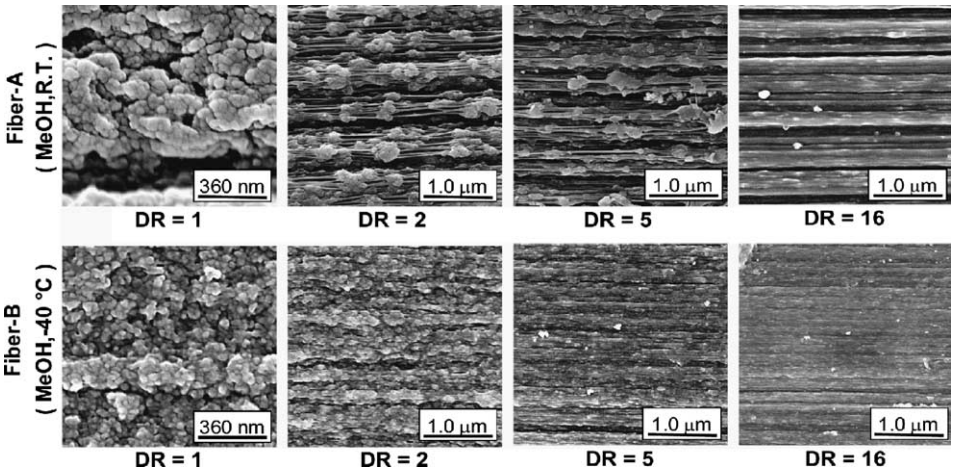

Fig. 4. SEM micrographs showing the changes in surface morphology during drawing for the draw ratio series prepared by the first-stage tensile draw at 140 °C and up to a DR of 16 for fiber-A (upper) and fiber-B (lower). The draw ratio is shown below each of the micrographs.

film shows a fairly sharp (110, 200) reflection ring. These facts suggest that the crystallinity of the fibers was significantly lower than that of the gel film, reflecting the differences in the solidification conditions. With increasing DR_t, the (110, 200) and (310, 020) reflections on the equator became gradually sharper, and their azimuthal intensity distribution became concentrated on the equator. The extremely high chain orientation is indicated by the circular reflection spots of the highly drawn samples with a $DR_{t,max} > 80$.

The crystalline chain orientation was evaluated by the Herman orientation function f_c determined by WAXD [27]. As the WAXD of PAN showed only the (110) and (200) reflections overlapped at around $2\theta = 17°$ with sufficient intensity, f_c was calculated from the azimuthal intensity distribution of this doublet assuming fiber symmetry. Fig. 6 shows the orientation function f_c vs. DR_t for the two-stage draw of the fibers and a gel film [6] carried out at an optimum T_d for each of them. The f_c of each sample increased rapidly with a DR_t in the lower range and reached $f_c = 0.98$–0.99 at a DR = 16 for both fiber-A and fiber-B and $f_c = 0.967$ for a gel film at an EDR = 16. These results deduced from the WAXD were qualitatively in agreement with the SEM observations of the changes in the surface morphology upon drawing (Fig. 4). At yet higher DR_t's, f_c increased slowly with DR_t, reaching a maximum value of $f_c = 0.995$–0.999 at DR_t's > 75, showing nearly perfect chain orientation for all samples. It is noted, however, that the draw efficiency, as evaluated from the f_c vs. DR_t, was higher for the fibers than for the gel film, reflecting the different initial morphologies (Figs. 2 and 5).

3.3. Development of tensile properties

Fig. 7 shows the tensile modulus vs. DR_t for the two-stage draw of UHMW-PAN fiber-A and fiber-B. The development of the modulus for the two-stage drawing of a gel film [6] is also shown for comparison. The second-stage draw of the samples

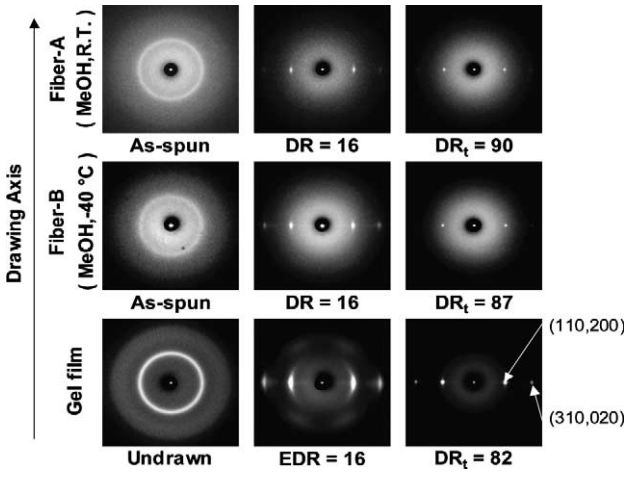

Fig. 5. WAXD patterns for the draw ratio series prepared from fiber-A (top) and fiber-B (middle). The WAXD patterns (bottom) for a draw ratio series from a gel film are also shown for comparison.

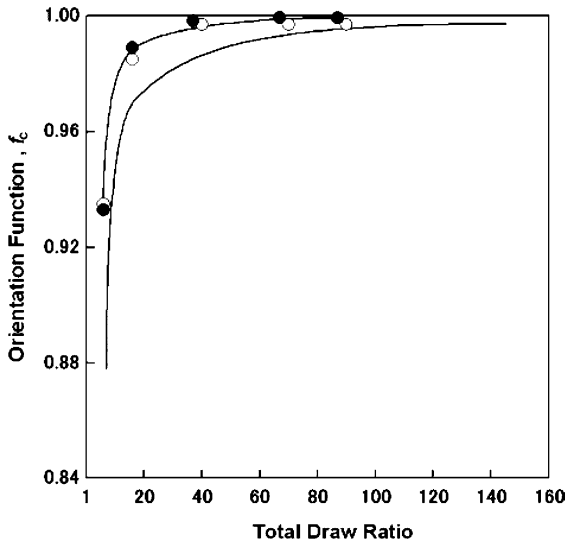

Fig. 6. Orientation function f_c as a function of DR_t for the two-stage drawing of fiber-A and fiber-B. The data for the drawing of a gel film are also included for comparison. The symbols are the same as those in Fig. 1.

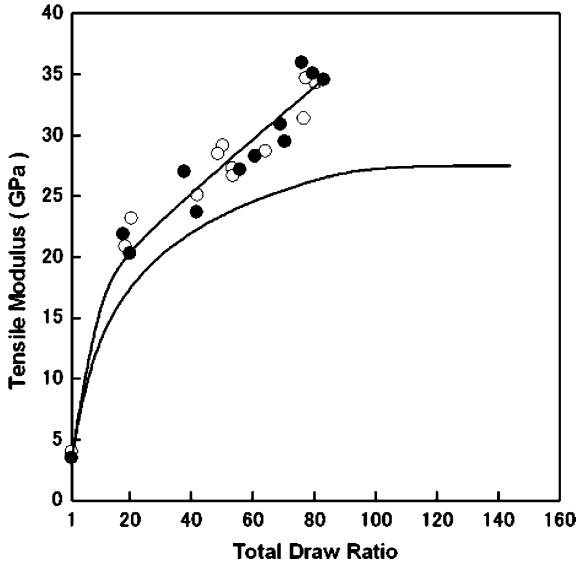

Fig. 7. Tensile modulus as a function of DR_t for the two-stage drawing of fiber-A and fiber-B. The data for the drawing of a gel film are also included for comparison. The symbols are the same as those in Fig. 1.

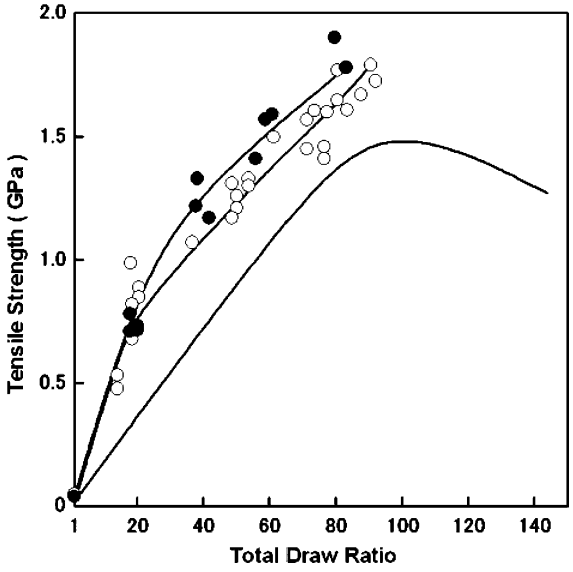

Fig. 8. Tensile strength as a function of DR_t for the two-stage drawing of fiber-A and fiber-B. The data for the drawing of a gel film are also included for comparison. The symbols are the same as those in Fig. 1.

previously drawn to a DR = 16 was made at an optimum T_d of 200–210 °C for each sample. The modulus of the drawn fibers increased more rapidly with DR_t than that of the gel film in the lower DR_t range, and reached a maximum value of 35 ± 1 GPa at around the highest DR_t of ~ 80. Although the gel film exhibited higher ductility than the fibers (Fig. 1), the tensile modulus increased only slowly with the DR_t at DR_t's > 40 and approached a maximum value of 28 GPa, which was lower than that achieved by the drawing of solution-spun fibers. This as well as the f_c vs. DR_t in Fig. 6 shows that less effective deformation occurred in the gel film.

One reason for the higher modulus achieved upon drawing of the fibers than upon that of a gel film is likely the better uniformity of the cross-sectional areas of the drawn fibers compared to that of the drawn gel films. Since stress concentration may occur at smaller cross-sectional areas, the observed modulus may be smaller than that expected for a uniform fiber having the same microstructure. Indeed, the variation of the cross-sectional area along a drawn product was $\pm 2\%$ for the fibers whereas that along a drawn gel film was $\pm 8\%$, as evaluated by SEM observations. Another reason for the lower maximum achieved modulus and the lower draw efficiency for the drawing of a gel film than for that of the fibers might be correlated with the formation of flaws at higher DR_t's, as observed by optical microscopy [6,8]. The maximum modulus of 35 GPa achieved for the two-stage drawing of UHMW-PAN solution-spun fibers is the highest ever reported for PAN fibers.

Fig. 8 shows the tensile strength vs. DR_t for the two-stage draw of UHMW-PAN fiber-A and fiber-B. The data for the drawing of a gel film are also included for comparison [6]. The strength of drawn fibers increased almost linearly with the DR_t, reaching a maximum of 1.8–1.9 GPa at the maximum achieved DR_t of 80–85. The strength of drawn gel films was significantly lower than that of the fibers, as also observed in the modulus vs. DR_t (Fig. 7). It was noted that the strength of the drawn gel films reached a maximum of ~ 1.5 GPa at around a DR_t of 100, and at yet higher DR_t's, the strength decreased with increasing the DR_t. In a previous study, such a decrease in the strength at higher DR_t's correlated with the formation of flaws observed by polarized optical microscopy [8].

The SEM observations of the as-spun fibers prepared by solution spinning into methanol coagulation baths kept at different temperatures (Fig. 2), the deformation modes (Fig. 3), and the morphological changes upon drawing (Fig. 4) revealed specific differences between fiber-A and fiber-B. However, the tensile modulus and strength at a given DR, as well as the maximum achieved tensile properties, were not significantly different between the two series of fibers prepared from fiber-A and fiber-B. The maximum achieved tensile modulus and strength were 35 and 1.8 GPa, respectively, for the drawing of solution-spun fibers. These values were 25 and 20% higher, respectively, than those previously achieved by drawing of a gel film of the same UHMW-PAN [6]. The enhancement of the tensile properties of PAN fibers has been achieved by controlling the morphology and uniformity of the fiber diameter of the initial fibers.

3.4. Crystal modulus of PAN

WAXD of oriented fibers is the most frequently used method for the measurement of crystal moduli of polymers [28,29]. The crystal modulus of a polymer in the chain direction is determined from the displacement of a meridional crystalline peak determined as a function of the stress applied along the fiber axis. A PAN fiber, however, shows only two or three sharp reflections on the equator and no sharp reflections on the meridian. Therefore, the common WAXD method

cannot be used for the measurement of the crystal modulus of PAN. Allen et al. [18] estimated an X-ray crystal modulus of PAN from the displacement of equatorial peaks instead of a meridional peak. They measured the changes of the (100) and (110) spacings of the hexagonal modification as a function of the stress applied along the fiber axis. Assuming that the volume of a PAN crystal does not change upon straining (i.e. Poisson's ratio $\mu=0.5$), they calculated the crystal strain in the chain direction as a function of the stress along the fiber axis. From the stress/strain curve thus obtained, they calculated an initial modulus of 28 GPa for a PAN crystal.

It was shown that a PAN chain takes a 3/1 helical conformation (isotactic sequences) and a planar–zigzag conformation (syndiotactic sequences) based on the two broad X-ray scatterings on the meridian analyzed by computer simulations [19,20]. Sakurada and Kaji [28] calculated the force required to stretch a polymer chain by 1% (f value) for various polymers, based on the elastic moduli of crystals in the chain direction and the cross-sectional area of a chain. They showed that the f values for various polymers are predominantly determined by the conformation of crystalline chains with a minor contribution from intermolecular interactions. By applying this rule to isotactic PAN having 3/1 helical conformation, the crystal modulus (E_h) was calculated to be 55 GPa [30] or 35 GPa [31].

The crystal modulus of PAN taking a planar-zigzag conformation (E_p GPa) can be estimated from the f value of a polyethylene crystal (f_{PE}). Assuming the crystal modulus of polyethylene in the chain direction of 235 GPa [28] and the unit cell constants of $a=0.740$ and $b=0.493$ nm with two chains penetrating a unit cell, the f_{PE} value is given by $f_{PE}=(E_{PE}\times10^9\ \mathrm{N/m^2}\times10^{-2})/(\text{number of PE chains/m}^2)=4.3\times10^{-10}$ N. Similarly, $f_{PAN}=(E_p\times10^9\ \mathrm{N/m^2}\times10^{-2})/(\text{number of PAN chains/m}^2)$. As the cross-sectional area of a PAN chain in a crystal is 3.2×10^{-19} m^2 [31], the number of PAN chains penetrating 1 m^2 is $1/(3.2\times10^{-19})=3.1\times10^{18}$. Thus, $E_p=f_{PAN}\times3.1\times10^{11}\mathrm{N}^{-1}$. Since $f_{PAN}=f_{PE}=4.3\times10^{-10}$ N, we obtain $E_p\approx130$ (GPa).

In a previous paper [6], we found that the intensities of the broad peaks at around $2\theta=36$ and 40° on the meridian, which were ascribed to the scatterings from the planar–zigzag and 3/1 helical sequences, respectively, changed with the DR of a sample. Fig. 9 shows WAXD meridional profiles of PAN fibers having different moduli of 9–28 GPa. The relative intensity of the scattering from the planar–zigzag sequences (around $2\theta=36°$) to the scattering from the 3/1 helical sequences (around $2\theta=40°$) increased with increasing the fiber modulus. This has an important implication concerning the characteristic nature of a PAN crystal. Unlike other polymers, the crystal modulus of PAN in the chain direction has no specific value and varies depending on the processing conditions of a sample reflecting the conformations of the crystalline chains.

As seen in Fig. 9, the meridional scattering for the high modulus fiber consists predominantly of the scattering from the planar-zigzag sequences at around $2\theta=36°$, suggesting that the modulus of such a fiber would approach a value expected for the planar-zigzag conformation. However, the maximum

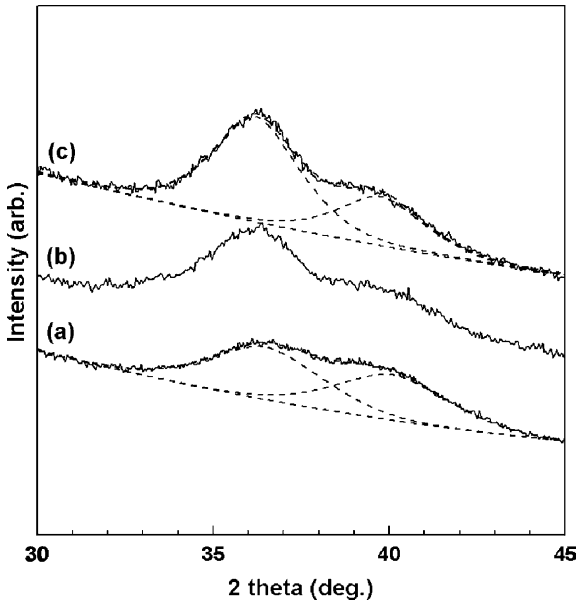

Fig. 9. WAXD meridional profiles for the fibers having different tensile moduli of 9 GPa (a), 17 GPa (b), and 28 GPa (c). Note that the intensity of the scattering from the planar–zigzag sequences at around $2\theta=36°$ increases with increasing the fiber modulus.

modulus achieved in this work was 35 GPa, significantly lower than that would be expected for the planar–zigzag conformation. This lower modulus is likely ascribed to the existence of kinks [19] and conformational disorder [32] along the chain as previously suggested by Liu and Luland [19] and Hu et al. [32].

3.5. Diameter dependence of the tensile strength

The effect of diameters on the tensile strength of fibers has been extensively studied. It has been shown that the ultimate strength of highly oriented UHMW-PE fibers [23–26] and carbon fibers [33,34] depends on the fiber diameters, which is consistent with the Griffith theory [35]. Pennings et al. [24,25] analyzed the size effect for a series of fully oriented UHMW-PE fibers having various fiber diameters. Their data fitted well into a modified Griffith equation shown below

$$\frac{1}{\sigma}=K_1D^{1/2}+K_2$$

where K_1 and K_2 are the constants, D, the fiber diameter, and σ, the tensile strength.

Fig. 10 shows the reciprocal of the tensile strength, $1/\sigma$, plotted against $D^{1/2}$ for three series of drawn PAN fibers having moduli of 20 ± 1 (series A), 27 ± 1 (series B), and 34 ± 1 GPa (series C). The data for Fig. 10 were obtained using fibers prepared from solution-spun fibers having different diameters obtained by spinning a 1 wt% solution using spinning dies with different capillary diameters. It is noted that the strength of PAN fibers that belong to a given series increases with decreasing the fiber diameter. As discussed based on the WAXD meridional profiles (Fig. 9), the crystalline chain

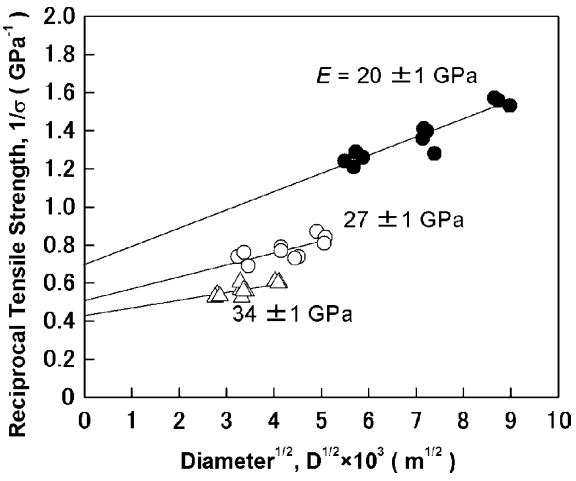

Fig. 10. Reciprocal tensile strength, $1/\sigma$, as a function of the square root of the diameter $D^{1/2}$ for three series of fibers having moduli of 20 ± 1 (●), 27 ± 1 (○), and 34 ± 1 GPa (△).

conformation of PAN varies depending on the sample modulus. Since, the fibers of a given series were prepared from the same solution (1 wt% solution) and had the same modulus, they might have a characteristic morphology responsible for the sample modulus. As seen from Fig. 10, the constants K_1 and K_2 change depending on the sample series, reflecting the characteristic morphologies of these sample series.

The value extrapolated to a zero diameter corresponds to the limiting tensile strength of a given series, in which no defects exist on the surface of the fiber. The strengths extrapolated to a zero diameter were 1.4 ± 0.1 GPa for series A, 1.9 ± 0.2 GPa for series B, and 2.4 ± 0.1 GPa for series C. As discussed, the conformation of crystalline chains varies with the fiber modulus (Fig. 9). Therefore, the strength estimated at a zero fiber diameter for each series corresponds to the limiting strength for the microstructure of each series. As the limiting strength estimated at a zero fiber diameter increases with the fiber modulus and the tensile modulus of 35 GPa achieved in this work is the highest ever reported for PAN fibers, the ultimate tensile strength is likely around 2.4 GPa for ultradrawn PAN fibers.

4. Conclusion

UHMW-PAN fibers spun from a dilute solution into methanol coagulation baths at different temperatures were uniaxially drawn by a two-stage tensile draw, and the development of the oriented morphology and tensile properties were studied. The results obtained were compared with those previously obtained for the drawing of gel films using the same UHMW-PAN. The initial morphology and deformation mode in the lower DR range were significantly influenced by the temperatures of the coagulation bath. However, the tensile properties at a given DR_t, as well as the maximum achieved ones, were comparable. The PAN fibers showing different moduli consisted of paracrystals in which the chains took different proportions of the planar–zigzag and 3/1 helical sequences. Unlike other polymers, therefore, the crystal modulus of PAN in the chain direction is not expressed by a specific value. The maximum achieved tensile modulus and strength at the break for the fibers (35 and 1.8 GPa, respectively) were significantly higher than those previously reported for the gel film (28 and 1.5 GPa, respectively). The modulus of 35 GPa is among the highest ever reported for PAN fibers. The significantly higher tensile properties achieved for the present fibers were ascribed to the increase of the planar–zigzag conformation in crystalline chains, the improvement in the uniformity of the fiber diameter (cross-sectional area) along the fiber axis and the decrease in fiber diameters. Indeed, it was noted that the tensile strength of fibers having comparable moduli increased with decreasing the fiber diameters. Furthermore, the reciprocal of the strength of the PAN fibers was proportional to the square root of their diameters, consistent with the Griffith theory. Extrapolation to the zero diameter yielded an ultimate tensile strength of 2.4 ± 0.1 GPa for the samples showing the maximum achieved tensile modulus of 35 GPa.

Acknowledgements

This work was partly supported by a Grant-in-Aid from the Ministry of Education, Culture, Sports, Science, and Technology of Japan (#17750207).

References

[1] Houtz RC. Text Res J 1950;20:786.
[2] Bajaj P, Agrawal AK, Dhand A, Kastruria N, Hansraj KN. JMS-Rev Macromol Chem Phys 2000;C40(4):309.
[3] Colvin BG, Storr P. Eur Polym J 1973;10:337.
[4] Rizzo P, Auriemma F, Guerra G, Petraccone V, Corradini P. Macromolecules 1996;29:8852.
[5] Kaji H, Schmidt-Rohr K. Macromolecules 2000;33:5169.
[6] Sawai D, Yamane A, Takahashi H, Kanamoto T, Ito M, Porter RS. J Polym Sci, Polym Phys Ed 1998;36:629.
[7] Bohn CR, Schaefgen JR, Statton WO. J Polym Sci 1961;55:531.
[8] Yamane A, Sawai D, Kameda T, Kanamoto T, Ito M, Porter RS. Macromolecules 1997;30:4170.
[9] Bashir Z, Rastogi S. J Macromol Sci, Part B: Phys 2005;44:55.
[10] Krigbaum WR, Tokita NJ. Polym Sci 1960;43:647.
[11] Smook J, Vos GJH, Doppert HL. J Appl Polym Sci 1990;41:105.
[12] Smith P, Lemstra PJ. Polymer 1980;21:1341.
[13] Smith P, Lemstra PJ, Pijpers JPL, Kiel AM. Colloid Polym Sci 1981;259:1080.
[14] Sen K, Bahrami SH, Bajaji PJ. MS-Rev Macromol Chem Phys 1996;C36(1):1.
[15] Sawai D, Hatakeyama K, Kanamoto T. Koubunshi Ronbunsyu 2002;59:274.
[16] Japan Exlan. US Pat. 4, 658, 004 (1987); Chem Abstr 102, 133462.
[17] Mitsubishi Rayon Co. Ltd. Jpn Kokai Tokkyo Koho, JP 6,335,821 (1988); Chem Abstr 110,59444.
[18] Allen RA, Ward IM, Bashir Z. Polymer 1994;35:4035.
[19] Liu XD, Ruland W. Macromolecules 1993;26:3030.
[20] Hu X, Johnson DJ, Tomka JG. J Text Inst 1996;86:322.
[21] Termonia Y, Meakin P, Smith P. Macromolecules 1985;18:2246.

[22] Kanamoto T, Porter RS. In: Kleintjens LA, Lemstra PJ, editors. Integration of fundamental polymer science and technology, vol. 3. London and New York: Elsevier Applied Science; 1989.
[23] Ohta T. Polym Eng Sci 1983;23:697.
[24] Smook J, Pennings AJ. J Mater Sci 1984;19:1359.
[25] Pennings JP, Vries AA, Ven JV, Pennings AJ, Hoogstraten HW. Philos Mag A 1994;69:267.
[26] Wagner HD. J Polym Sci, Polym Phys 1989;27:115.
[27] Alexander LE. X-ray diffraction methods in polymer science. New York: Wiley; 1969.
[28] Sakurada I, Kaji K. J Polym Sci, Part C 1970;31:57.
[29] Nakamae K, Nishino T, Takagi S. J Macromol Sci, Phys 1991;30:47.
[30] Allen RA, Ward IM, Bashir Z. Polymer 1994;35:2063.
[31] Sawai D, Yamane A, Kameda T, Kanamoto T, Ito M, Yamazaki H, et al. Macromolecules 1999;32:5622.
[32] Rizzo P, Auriemma F, Guerra G, Petraccone V, Corradini P. Macromolecules 1996;29:8852.
[33] Reynolds W, Sharp J. Carbon 1974;12:103.
[34] Matsuo Y, Yasuda K, Kimura S. J Ceram Soc Jpn 1990;98:389.
[35] Griffith AA. Philos Trans R Soc London, Ser A 1920;221:163.